Numerical Study of Noise Reduction on Looped Propeller Blades with Bio-inspired Tubercles

Justin du Plessis, Abdessalem Bouferrouk, and Alessandro Pontillo

School of Engineering, University of the West of England, Bristol, BS15 4AD, UK

Abstract This paper investigates the effect of looped propeller blades with bio-inspired sinusoidal leading-edge tubercles on the tonal noise generated. CFD simulations are conducted using ANSYS Fluent, utilising a Detached Eddy Simulation flow model combined with a Ffowcs Williams Hawkings model for acoustics. Further RANS simulations were conducted for performance simulations in static and forward flight conditions. The findings show that the baseline looped propeller was able to reduce the tonal noise by up to 3.49dB at the blade passing frequency, in comparison with a reference standard propeller. It is also found that all the tested tubercle variations on the looped design can further reduce the noise at the tonal harmonics by 0.98dB at the blade passing frequency. The results further show that the looped propellers and their tubercle variations reduced the maximum thrust generated but were able to reduce the input power required at all tested velocities. The findings demonstrate the potential of bio-inspired looped propellers for noise reduction on eVTOLs and UAVs operating in urban environments.

Keywords: Propeller Noise; Aeroacoustics; Looped Propeller; Biomimicry; Tubercles

1. Introduction

Recent years have seen a stark increase in the development of eVTOL aircraft and drones, particularly for operation within urban environments. A common design feature shared amongst the range of designs currently being implemented and developed is the use of electrically driven propellers for propulsion. Such propellers provide high propulsive efficiency and can be easily integrated with electric motors. One of the main drawbacks of propellers, however, is the amount of aerodynamic noise generated during flight, which becomes particularly sig- nificant when operating within urban environments.

Aerodynamic noise is the result of small but rapid and unsteady pressure fluctuations, due to the interaction between the fluid and the surface of a noise source. These aerodynamic noise sources are typically split into two groupings, tonal noise and broadband noise.

Tonal noise tends to present itself as large sound pressure level (SPL) spikes at discrete frequencies across the audible frequency range. For propellers and rotors, the discrete tones are multiples of the blade passing frequency (BPF). Tonal noise occurs because of interactions between the rotor and the tip vortex formations, known as blade vortex interactions (BVI). Broadband noise is distributed across the entire captured frequency range, and forms as a result of small-scale random disturbances on the surface of the noise source (Xiran et al., 2022), e.g. small-scale eddies in a turbulent boundary layer, or eddies in a separated flow. In the current paper, the focus is on reducing tonal noise.

Although both tonal and broadband noise contribute to form a total noise signature, previous research studies have shown that the tonal noise is the largest component of noise produced by a propeller, and has a significant effect on human comfort e.g. Cai, Qi, & Zhang (2012) and Patil, Borole & Sanap (2013). Numerous methods have been suggested to reduce the tonal noise, one such method is to change the tip geometry of the propellers to alter the noise created by BVI (Hanson et al., 2022). Another extreme is to completely redesign the general shape of the propellers, in the form of a looped propeller. Previous research has shown that the usage of a looped blade is able to create large reductions in the noise generated from tip vortices, but at a cost to the peak thrust and efficiency of the propellers e.g. Shima, Sun, Liu, Yonezawa, & Kaneko, (2024), Shima & Tsutsumi, (2023).

Bio-mimicry features have also been explored in previous research for their ability to reduce noise generated without creating large negative impacts on the performance of pro pellers. Trailing-edge serrations have been studied extensively including applications to wind turbines and UAVs for their ability to create noise reductions with small effects on the efficiency e.g. Hsiao, Zhenbo, Kian, Jinlong, & Heow, (2019), Zang et al., (2023). Research into trailing-edge finlets, inspired by owls, has shown potential to reduce noise generated by lift- ing the energetic turbulent eddies away from the trailing edge (Wilkins & Bouferrouk, 2023). Another researched feature is the implementation of leading-edge tubercles as found on the pectoral fins of humpback whales. Seminal research by Fish and Lauder (2006) found that tubercles can reduce flow separation by generating small contra-rotating vortices on the surface air- foils. Furthering on the research, Colpitts and Perez (2023) found that tubercles were able to reduce the induced drag created by the tip vortex formation on a rotor blade. In this paper, we investigate the role of tubercles for noise reduction on propellers.

The present paper builds on recent research by the authors which found that the looped propeller blades were able to reduce the overall sound pressure level (OASPL) by up to 10dB vertically above and below the propeller, though with a loss of propulsive efficiency of up to 15% depending on the propeller's RPM (du Plessis & Bouferrouk, 2024). More specifically, the paper aims to combine the looped propeller concept with leading- edge tubercles to investigate the tubercles potential to further the looped propeller's noise reduction effects, and to see if they could reduce the propeller blade's drag and hence reduce power required. The research makes usage of high fidelity Detached Eddy Simulations (DES) using ANSYS Fluent (version 2023 R1) for flow simulation, combined with the Ffowcs Williams Hawkings (FW-H) acoustic analogy for calculating acoustics data in the far-field at set receiver points.

2. METHODOLOGY

2.1 Propeller Designs

The reference (non-looped) propeller used for this research is based on the design by Hanson et al. (2022). The two-bladed propeller geometry as presented in Figures 1 and 2 is characterised by a hub section, a constant chord length, and a constant pitch-to-diameter ratio (diameter = $0.254m$). The simple blade geometry was selected as it allowed for comparisons with variant propellers to be made without having to consider the effects created by the sweep and tapering of blades.

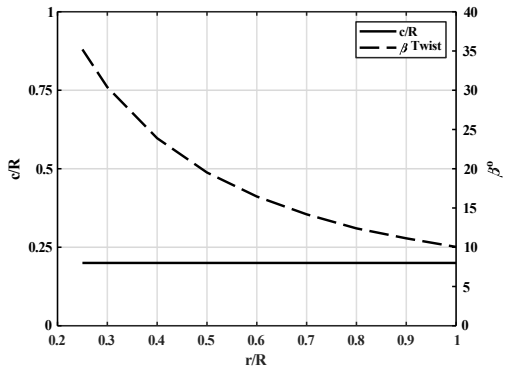

Figure 1: Reference Propeller Constant Chord, Variable Twist Distribution

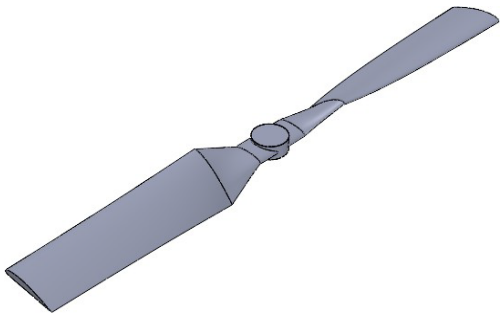

Figure 2: Reference Propeller CAD Geometry

The looped propeller was created using the same constraints as was done in previous research (du Plessis & Bouferrouk, 2024), in which the diameter was kept constant while the chord length was halved, to maintain a comparable surface area and solidity. Figure 3 shows the looped propeller geometry.

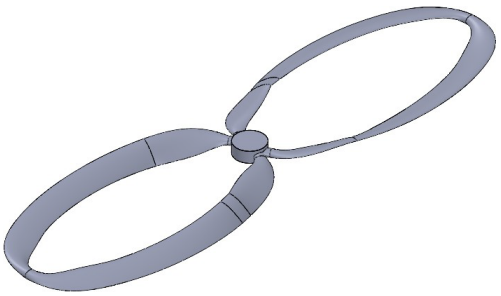

Figure 3: Looped Propeller CAD geometry

The tubercle dimensions were taken from research done by Fahad and Talha (2019). These tubercle dimensions were selected as they were shown to reduce drag on the $0.254m$ diameter blades, hence they are likely to have a similar effect on the equal-diameter blades used in this study. Table 1 shows the configurations of three variants of the sinusoidal tubercles, with the wavelength (λ) as a function of span (s) and the amplitude (A) as a function of the chord length (c).

Table 1: Tubercle Shapes

Variant	λ	A
T1	0.0425s	0.1c
T2	0.085s	0.1c
T3	0.03s	0.2c

Figures 4-6 show the shape of the tubercles on the leading edge of the looped propeller blades. The Tubercles were positioned to start at 0.25R and end at 0.9R to allow enough space for the loop connection to occur undisturbed.

Figure 4: T1 Variant

Figure 5: T2 Variant

Figure 6: T3 Variant

2.2 Numerical Setup

Steady-state RANS simulations were used to resolve the flow field around the propellers, and to estimate the thrust and power performance of the propellers in static and forward flight conditions. Following this, transient acoustic simulations (based on DES) were conducted after being initialised from the steady-state solutions. The transient acoustics simulations were conducted for 15 rotations at 5^o of rotation per time step. The FW-H acoustics analogy was selected, as used previously (du Plessis & Bouferrouk, 2024), since it allowed for the acoustics calculations to be decoupled from the mesh. This decoupling allows for acoustics data to be obtained at receiver points in the far field outside of the mesh region. Table 2 shows the solver setup for the simulations, and Figure 7 shows the locations of the eight receivers used for the acoustics (a separation angle of 10 degrees between the receivers).

Table 2: Numerical Setup for Flow and Acoustics Simulations

Solver Setting	Acoustics	Performance
Time Advancement Method	Transient-Fixed	Steady State
Time Step Size (s)	1.19e−4	-
Rotation Method	Mesh Motion	Frame Motion
Solver Type	Pressure Based	Pressure Based
Velocity Formulation	Absolute	Absolute
Viscous Model	Delayed Detached Eddy Simulation (DDES)	-
RANS Model	kω-SST	kω-SST
Acoustics Model	FW-H	-
Spatial Discretisation-Pressure	Second Order	Second Order
Spatial Discretisation-Momentum	Second Order	Second Order

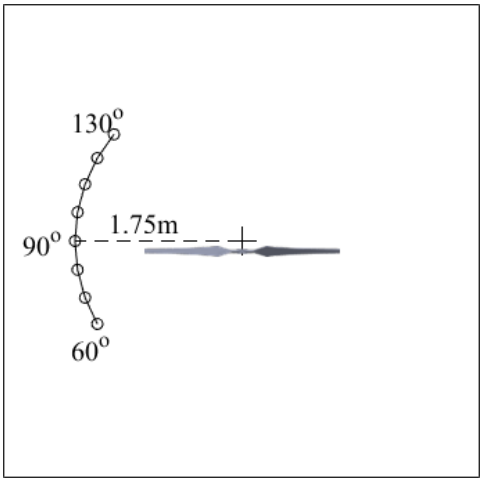

Figure 7: Receiver Locations, O denotes receiver locations

Due to limitations on computational facilities available, this work makes use of DES which is a hybrid turbulence modeling approach that combines Reynolds-Averaged Navier- Stokes (RANS) and Large Eddy Simulation (LES) methods ; using RANS in attached boundary layer regions and LES in separated flow areas. To address potential issues with standard DES, the current work employed a Delayed Detached Eddy Simulation (DDES) approach, which introduces a delay function to prevent premature activation of the LES mode in attached boundary layers. This helps ensure the RANS model (kω-SST in this study), is used appropriately in boundary layer regions, while transitioning to the LES approach only in areas with strong flow separation.

ANSYS Meshing was used to generate a hybrid mesh within the fluid domain. Tetrahedral elements were used in the bulk of the volume while switching to hexahedral elements within the boundary layer region on the surface of the propellers. The hexahedral elements were generated from the 99% boundary layer height and allowed to shrink towards the propeller wall with 14 layers, after each simulation, the y^+ values were plotted on the surface of the propeller to ensure a $y^+ < 5$ was obtained. Figures 8 and 9 show the dimensions of the cylindrical domain and the mesh used for the computations respectively. Figure 10 and 11 shows the hexahedral elements created to capture the boundary layer flow.

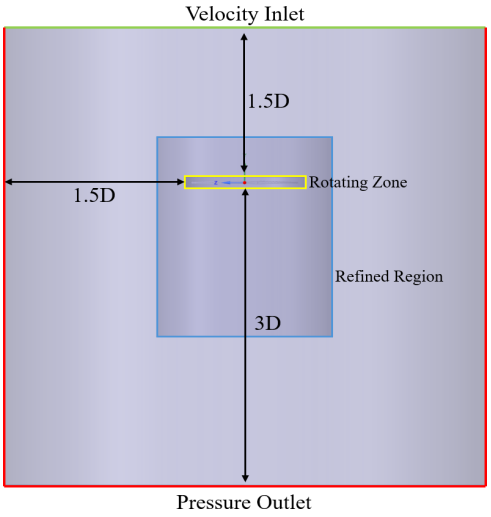

Figure 8: Domain and Boundary Conditions

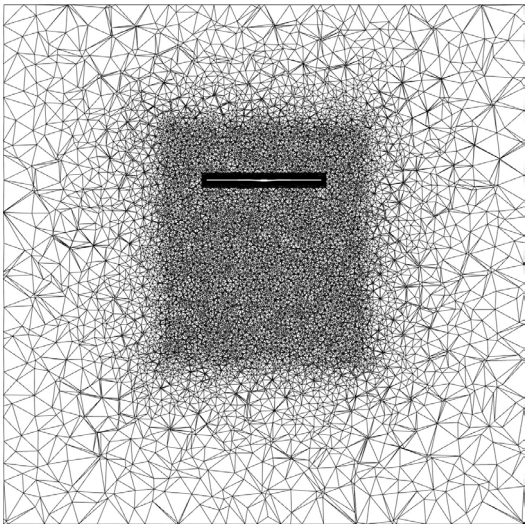

Figure 9: Hybrid Mesh

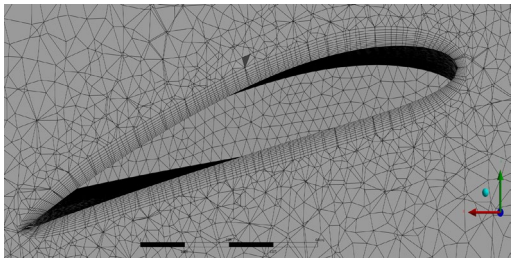

Figure 10: Reference Propeller Inflation Region

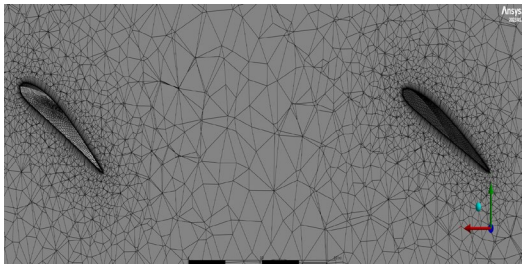

Figure 11: Looped Propeller Inflation Region

2.3 Propeller performance parameters

Propeller performance is evaluated as a combination of thrust (T), torque (Q), power required (P), and efficiency (η) in both static and forward flight conditions. For comparison, these values are typically presented as non-dimensionalised coefficients. During simulations the atmospheric pressure, density, and temperature were set to ISA sea-level conditions.

The thrust coefficient (C_T), torque coefficient (C_Q) and power coefficient (C_P) are calculated, using the rotations per second (n) and the propeller diameter (D), as follows:

$$C_T \quad \frac{T}{\rho n^2 D^4} \tag{1}$$

$$C_Q \quad \frac{Q}{\rho n^2 D^5} \tag{2}$$

$$C_P = 2\pi C_Q \tag{3}$$

When the propeller is operating in forward flight conditions, an advance ratio (J) needs to be calculated to account for the freestream velocity (V_∞) of fluid. When the advance ratio is calculated it also allows for efficiency (η) to be calculated.

$$J = \frac{V_\infty}{nD} \tag{4}$$

$$\eta = \frac{C_T J}{C_P} \tag{5}$$

Because obtaining a value for efficiency requires a freestream velocity, it can only be used for evaluation in forward flight conditions. A similar performance can be made in static conditions by calculating the figure of merit (FOM). The process is shown in equations 6-8, where Ω = rotational speed (rad/s), A = propeller disk area (m^2) and R = propeller radius (m):

$$FOM = \frac{P_{ideal}}{P} = \frac{\frac{3}{2}}{\sqrt{2}} \frac{T_0}{C_P} \tag{6}$$

$$C_{T_0} = \frac{T}{\rho A(\Omega R)^2} \tag{7}$$

$$C_{P_0} = \frac{P}{\rho A(\Omega R)^3} \tag{8}$$

2.4 Numerical Validation

The numerical approach was validated by comparing the reference propeller's thrust coefficient and SPL obtained at the first BPF with the experimental data obtained by Hanson et al., (2022) as shown in tables 3 and 4.

Table 3: C_T Validation

Tip Mach Number	C_T (Hanson et al., 2022)	C_T Numerical	% Error
0.116	0.0994	0.09702	2.41
0.154	0.1026	0.09747	4.97
0.193	0.1063	0.09767	8.10
0.231	0.1083	0.9752	9.92
0.270	0.1108	0.10165	8.28

Table 4: Acoustics Validation of SPL (dB), at 7000RPM, V_∞ = 8m/s

Receiver	BPF1 dB (Hanson et al., 2022)	BFP1 dB Numerical	ΔdB
80	65	66.17	1.17
90	67.5	65.61	1.89
100	68	65.26	2.74

When the results of the reference propeller were compared, it was determined that although the CFD under-predicted the C_T, the results were all within 10% of the experimental values and followed the correct trend. Alongside this, the acoustics values obtained were all within 3dB.Consequently, it was decided that the simulations were adequate.

3. RESULTS

The results are separated into three subsections for acoustics, propeller performance and flow behaviour.

3.1 Acoustics Results

Acoustics simulations were conducted with all the propellers rotating at 7000 RPM and a freestream velocity of $8m/s$, to match the validation conditions for the reference propeller. Analysis was first done by comparing the maximum sound pressure level (SPL) at the first blade passing frequency (BPF) spike created by each of the propellers. Table 5 shows the max SPL value at the BPF obtained from each propeller at the 90^o receiver location.

Table 5: Propeller Max SPL at receiver 90^o

Propeller	SPL at BPF1 (dB)
Reference	65.61
Looped	62.12
T1	61.14
T2	61.18
T3	61.73

The findings showed that the looped propeller was able to achieve a 3.49dB reduction in the SPL value at the BPF, while all three of the looped tubercle variations were able to further reduce the noise tonal noise spike, with T1 being the quietest at 61.14 dB.

Figure 12 shows the captured noise spectrum for the reference propeller (receiver 90^o). The first tonal BPF spike can be seen at the frequency of 233Hz, with BPF2 and BPF3 seen at 466Hz and 700Hz respectively. The BPF spikes were used to investigate the impact the geometry had on the noise created by the tip of the propellers as they passed the receiver locations at each rotation. Although other harmonic spikes can be seen in the graphs, BPF1, BPF2, and BPF3 were selected as the main tones due to their larger magnitudes compared to the other harmonic spikes.

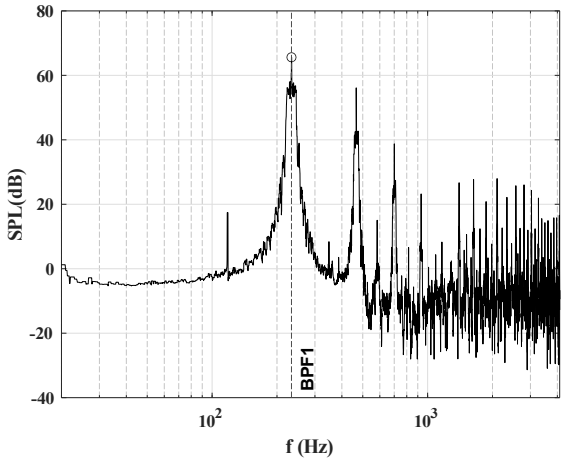

Figure 12: Reference Propeller Noise Spectrum at 90^o Receiver Location

Figures 13-16 show the captured noise spectra for the looped propeller and its tubercle variants at the 90^o receiver location. All the spectra again show the BPF spikes with the largest SPL value occurring at BPF1 for all the propeller variants. All variants experienced SPL reductions at the BPF spikes 2 and 3. The largest reductions occurred be- tween 100Hz and 1000Hz, showing that the looped propellers are most effective at reducing noise in the low-frequency ranges.

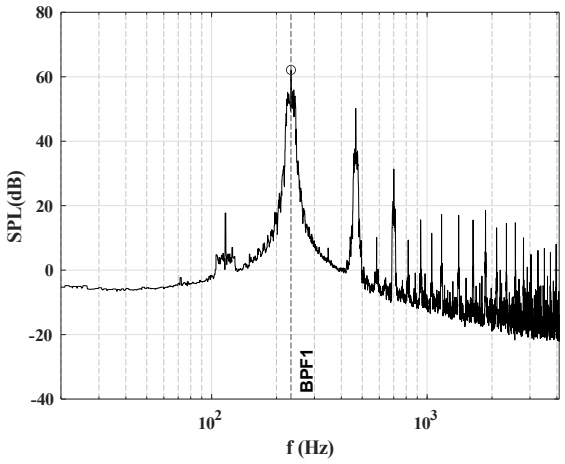

Figure 13: Baseline Looped Propeller Noise Spectrum

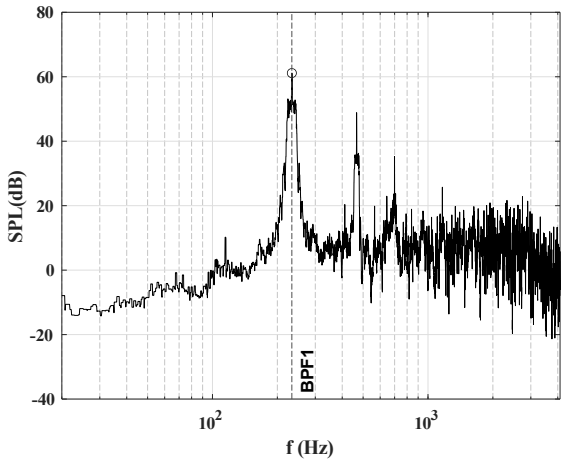

Figure 14: T1 Noise Spectrum

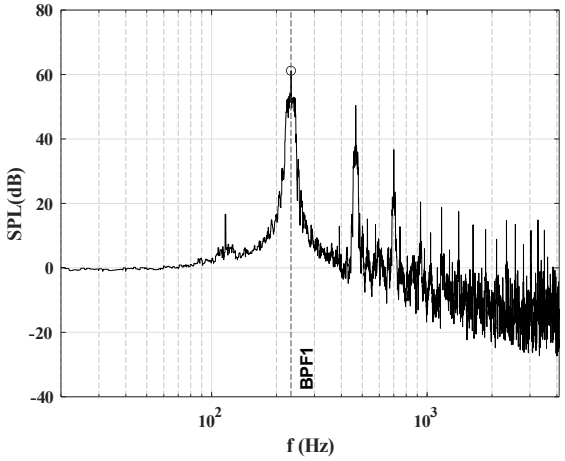

Figure 15: T2 Noise Spectrum

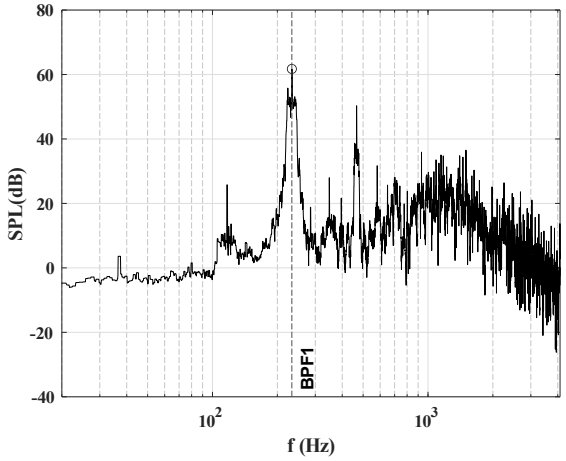

Figure 16: T3 Noise Spectrum

To gain an understanding of how the noise changes across the entire captured frequency spectrum, the overall sound pressure levels (OASPL) were plotted for all propellers, at each of the receiver locations. This allowed to compare not only the propeller variants but also allowed for gaining insights into the directionality of the noise emitted from the pro- pellers.

Figure 17 shows the averaged OASPL value obtained from all the receivers for the different propellers. The bar chart clearly shows the large reductions that the looped propeller blades were able to achieve, with the T1 variant achieving the largest reduction.

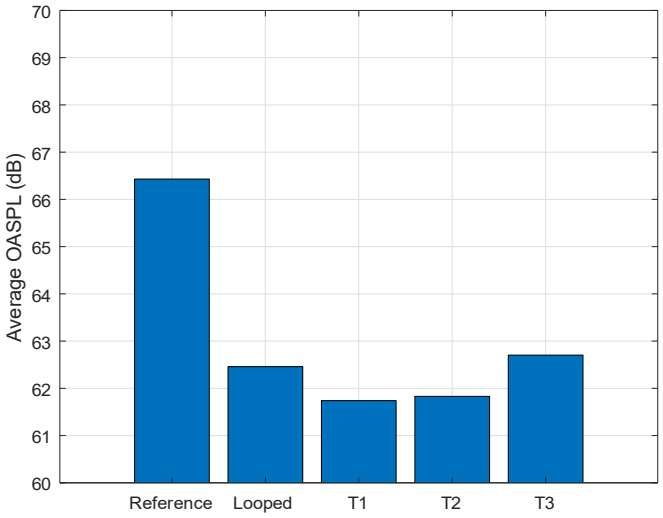

Figure 17: Average OASPL from 8 Receivers for Different Propeller Geometries

Figure 18 shows the individual OASPL values from each of the propellers at the receiver locations. It is seen that the looped propeller and all its variants achieved large reductions in OASPL, at all receiver locations, when compared with the reference non-looped propeller.

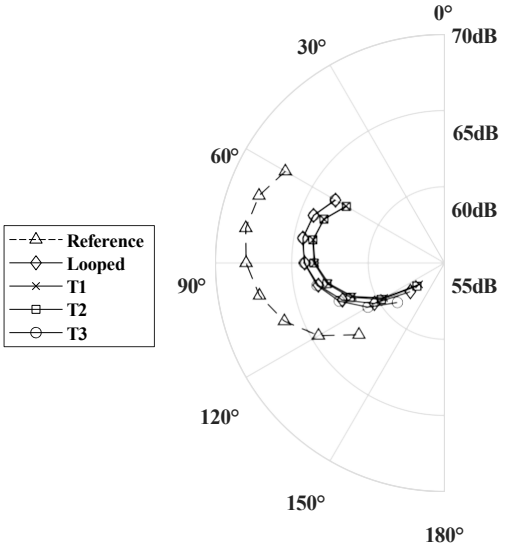

Figure 18: OASPL Values at receiver locations from all Propellers

Figure 19 expands on the data in Figure 18 by focusing on the tubercle variations. The data shows that T1 and T2 both consistently achieved very similar levels of noise reduction at all receiver locations. Furthermore, T1 and T2 both consistently achieved larger noise reductions than T3. Since T1 ultimately had the largest noise reductions, T1 was plotted against the reference propeller and the standard looped propeller in Figure 20, to compare its impact.

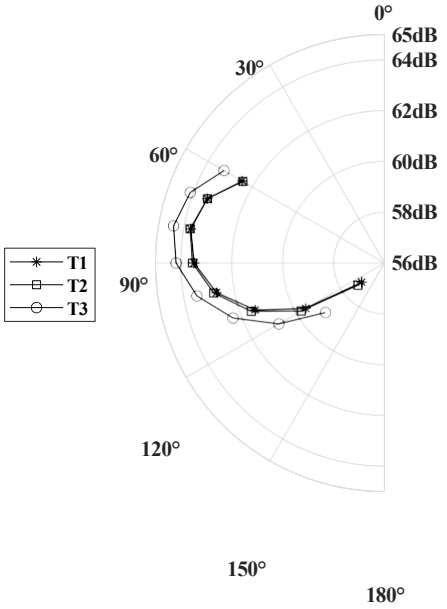

Figure 19: Tubercle Variants OASPL

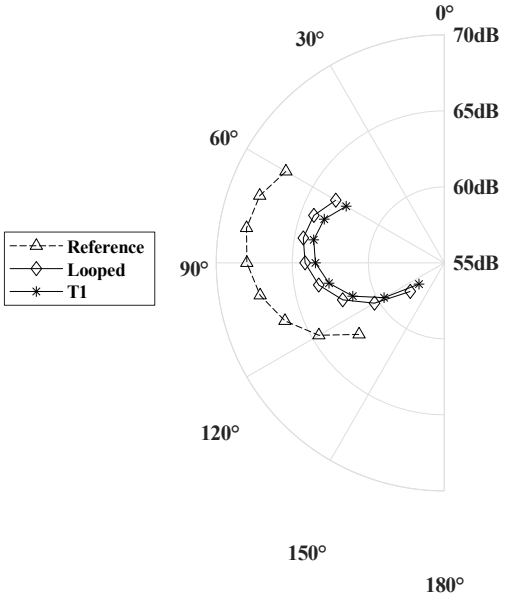

Figure 20: OASPL Values for Reference, Looped and T1

Further analysis was done by plotting contours of the acoustic pressure fluctuations on the surface of the propeller blades in Figures 21 - 23. These contours assist in gaining an insight into where on the propeller blade the noise originates from and how it changes between the different variants.

Looking at the reference propeller (Figure 21), the largest pressure fluctuations occur on the leading edge and the tip of the blade, with a relatively uniform distribution across the entire blade.

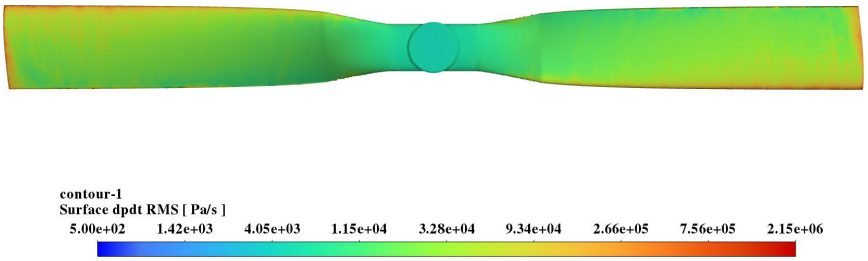

Figure 21: Reference Propeller Acoustics Pressure Fluctuations

The pressure contour for the standard looped propeller is shown in Figure 22. When compared with the reference propeller (Figure 21) the small pressure fluctuations are significantly reduced at the hub section, and smaller reductions are found along the rest of the blade up till the tip region.

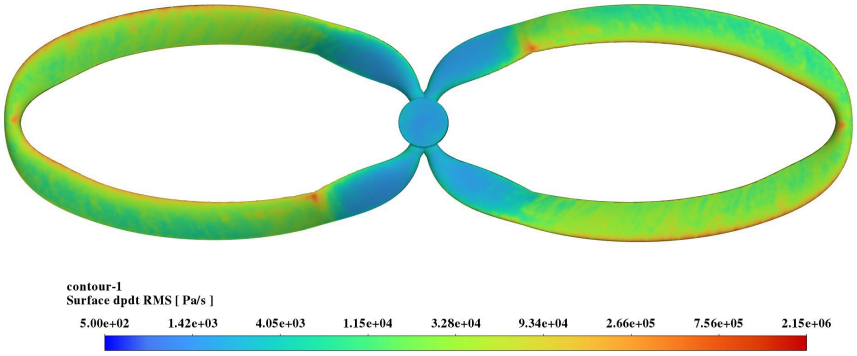

Figure 22: Looped Propeller Acoustics Pressure Fluctuations

The behaviour of acoustic pressure fluctuations was then further analysed using T1 as in Figure 23. Similar large reductions are again found in the hub region. The pressure fluctuations show reduced amounts between and behind the troughs of the leading-edge tubercles and further reductions in the magnitude of the fluctuations at the tip. Although there are some small concentrations of higher magnitudes at the inboard section of the blade, in general the magnitude of the magnitude of the acoustics pressure fluctuations has decreased over most of the blade.

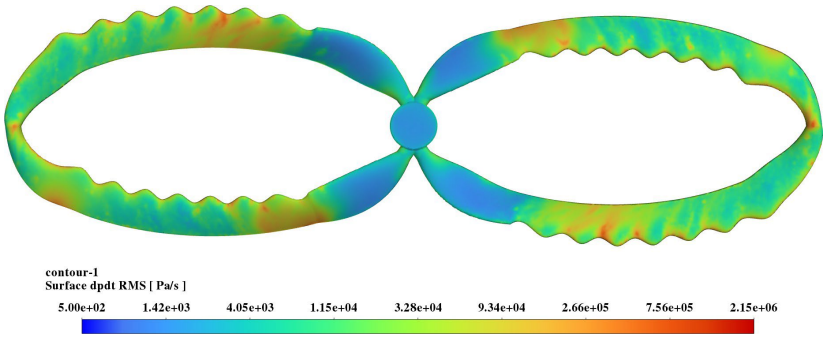

Figure 23: T1 Acoustics Pressure Fluctuations

3.2 Performance Results

Figure 24 shows the static C_T results, while Figure 25 shows the forward flight C_T results for all propellers. When looking at the results, the trend for the looped propeller is very similar to what was found in previous research (du Plessis & Bouferrouk, 2024), with a 19% to 23% reduction in C_T across the entire RPM range in both test conditions when compared with the reference propeller. The simulations also show that none of the tubercle modifications increased C_T and that they were all detrimental to the propeller's C_T performance.

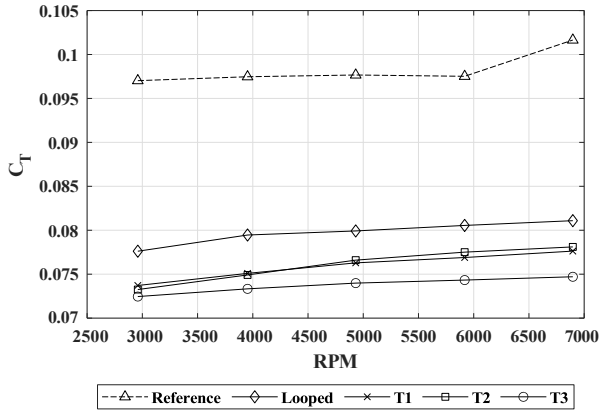

Figure 24: Static C_T Comparison

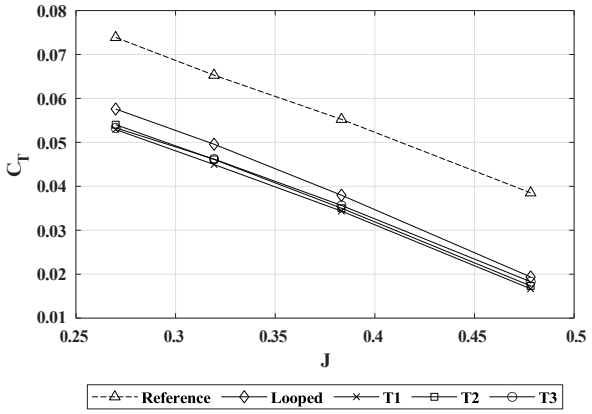

Figure 25: Forward Flight C_T Comparison, $V_\infty = 8m/s$

Further looking into the static results (Figure 24), T1 and T2 yielded very similar losses in C_T (5% reduction) when compared to the standard looped propeller across the whole RPM range. This is in contrast with T3 which started with a similar C_T reduction as T1 and T2 at low RPM but then increases to an 8% reduction at 6897RPM when compared with the baseline looped propeller. Looking at the forward flight conditions (Figure 25) it can be seen that the C_T losses for T1, T2, and T3 are consistently smaller when compared to the baseline looped propeller and are largest at the low advance ratios, with T3 also performing in line with the other tubercle looped blade variants.

The input power coefficient C_P results are presented in Figures 26 and 27. The findings show that in static conditions (Figure 26) the looped propeller and its tubercle variations, T1 and T2, were able to achieve significant reductions in C_P when compared to the reference pro- peller.T3 shows that it started with a higher C_P up till 4000RPM, but was able to achieve further reductions at the higher RPMs. The standard looped design achieved a 9% reduction at 2959RPM and improved to a 14% reduction in C_P at 6897RPM. This trend again holds true when looking into the forward flight results (Figure 27), where the baseline looped design reduced the C_P by 16% when compared to the reference non-looped propeller across the range of advance ratios.

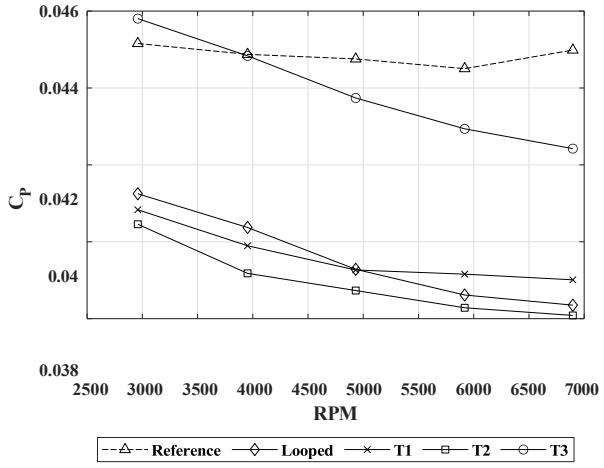

Figure 26: Static C_P Comparison

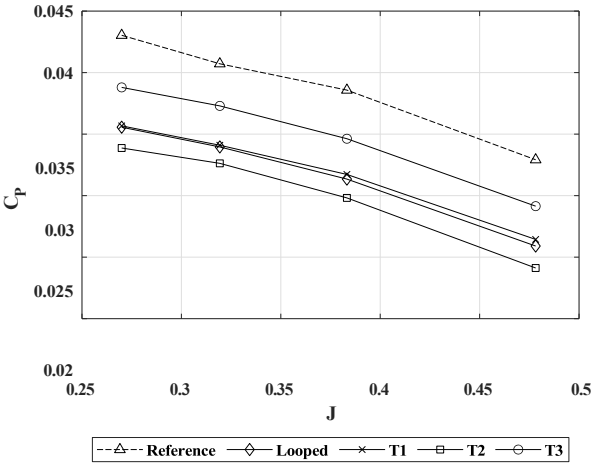

Figure 27: Dynamic C_P Comparison, $V_\infty = 8m/s$

The overall effect of the changes to C_T and C_P can be seen when looking into the Figure of Merit and efficiency graphs in Figures 28 and 29 respectively. In static conditions the

standard looped propeller experiences a 20% drop in FOM at 2959 RPM and a 17% drop at 6897RPM when compared to the reference propeller. Looking at the efficiency (Figure 29) it can again be seen that the standard looped propeller suffers a 4.5% reduction in efficiency at low advance ratio and a 28% reduction at high advance ratios (above J = 0.38). This suggests that the looped propeller can achieve similar efficiency at high RPMs and that it could be viable specifically in forward flight cruise scenarios, where noise reduction is a main priority.

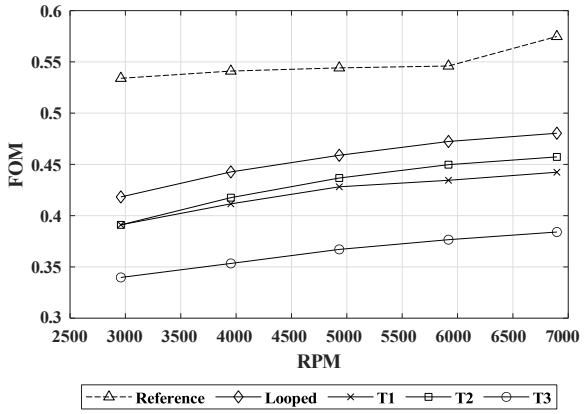

Figure 28: FOM Comparison

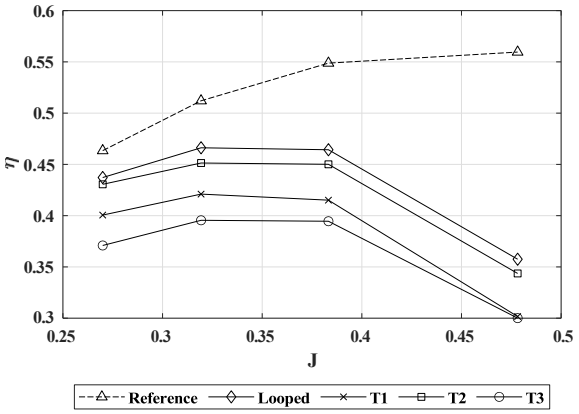

Figure 29: Efficiency Comparison, $V_\infty = 8m/s$

Adding the tubercles to the looped propeller results in reductions to FOM and efficiency in static and forward flight conditions. T3 consistently suffered the largest reduction in FOM, with a 20% average reduction when compared with the baseline looped propeller. T1 and T2 experience much smaller reductions in FOM when compared to T3 but still have a lower FOM when compared to the baseline looped propeller (7.5% average reduction).

3.3 Flow Behaviour

Changes to the flow behaviour were studied with a focus on changes to the tip vortex formation, and changes to the turbulent kinetic energy on the upper surface of the propeller blades. Figures 30 - 32 show the tip vortex formation, on the reference non-looped propeller, the baseline looped propeller and the T1 variant respectively.

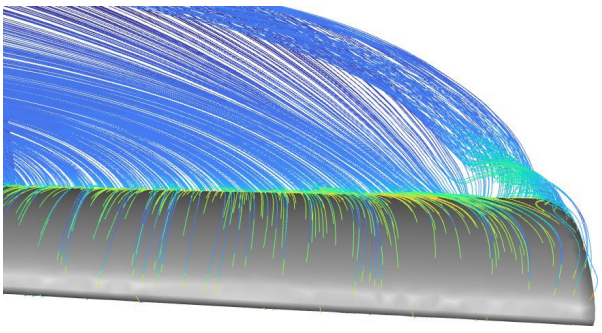

Figure 30: Reference non-looped Propeller Tip Vortex

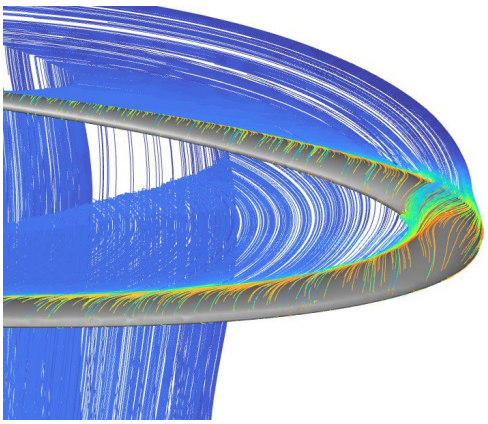

Figure 31: Baseline Looped Propeller Tip Vortex

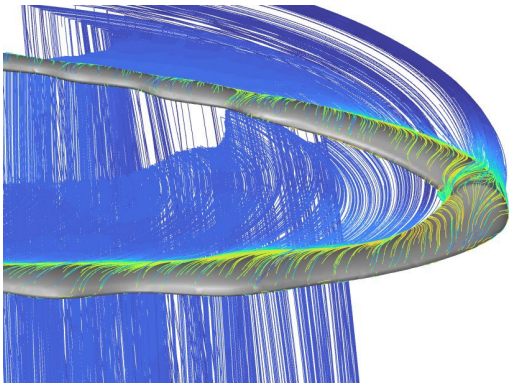

Figure 32: Looped T1 Variant Tip Vortex

Looking into the reference propeller's streamlines (Figure 30), a single sightly bound vortex is formed at the tip of the propeller. This differs from the baseline looped and T1 variants, in which no obvious concentrated tip vortex formation can be seen. It can also be seen that the flow in the wake of the looped and T1 variants diffuse and become more uniform earlier than seen on the reference blade.

These findings correlate with the findings of the previous research done by the authors (du Plessis & Bouferrouk, 2024) and the findings from research done by Shima et al. (2023), in which the authors found reductions in the formation of tip vortices on looped propellers when compared to a standard design.

Figures 33-35 show the turbulent kinetic energy (TKE) distribution on the upper surface of the reference, baseline looped and T1 variant blades respectively. The results for the reference propeller (Figure 33) show that the TKE is spread uniformly from 25% radius to the tip of the blade, with the largest magnitude occurring at the tip of the blade.

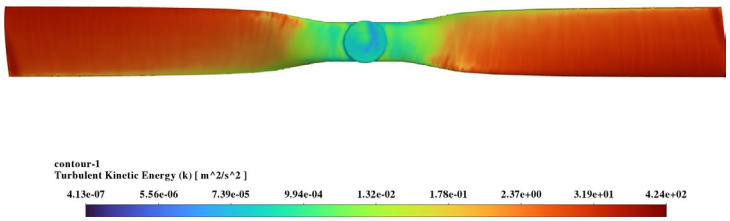

Figure 33: Reference Propeller TKE

The baseline looped design (Figure 34) shows huge reductions in the TKE formation on the blades when compared to the reference design. The contour shows that the formation of TKE is more concentrated towards the tip of the blade and is effective at reducing the turbulence encountered over the rest of the blade span.

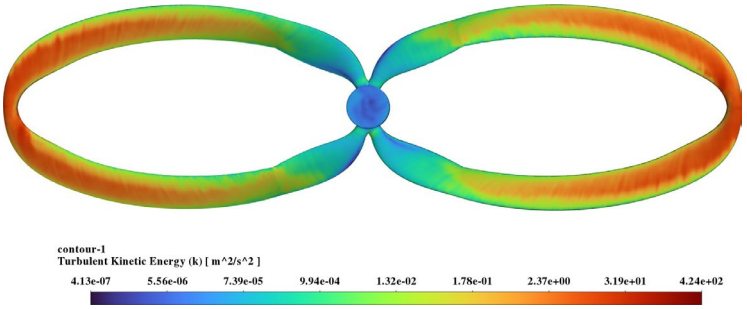

Figure 34: Baseline Looped Propeller TKE

For the T1 variant (Figure 35) shows that the variant is able to significantly reduce the amount of TKE formation over the blade span when compared to the reference propeller. As seen with the standard looped propeller (Figure 34) the largest magnitudes of TKE are localised at the tips of the propeller. The addition of the leading-edge tubercles has also created small concentrations of TKE between and slightly behind the troughs of the tubercles.

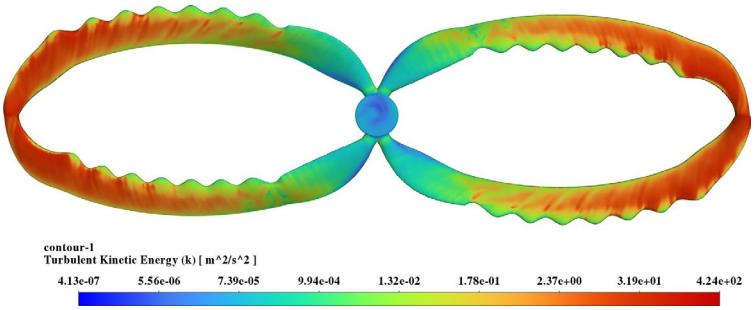

Figure 35: T1 Variant TKE

Overall, the changes to the tip vortex formation and TKE distribution on the blade, are possibly what leads to the reduction in drag for the propeller blades, which results in the obtained reductions in C_P.

4. Conclusions and Further Work

This study's investigation into the effect of leading-edge tubercles on a looped propeller blade demonstrates the potential of such designs and modifications for reducing tonal noise. CFD simulations have been conducted using ANSYS Fluent, utilising a Detached Eddy Simulation flow model combined with a Ffowcs Williams Hawkings model for acoustics. The acoustics results show that the looped propeller blade can offer large reductions in noise when compared to a traditional reference blade. In addition, all the tested sinusoidal leading-edge tubercles were able to further reduce the noise generated from the looped propeller blades at the blade passing frequencies. T1 and T2 were also able to further reduce the noise when comparing the OASPL values, but T3 was unable to improve the OASPL noise reduction. As these noise reductions were simulated using DDES with a k-ω SST RANS model, the noise reductions found should be attributed to tonal noise reductions, while the effect on the broadband noise is still unknown, as the model will not have fully resolved the effects of vortex shedding within the boundary layer.

The tradeoff to this noise reduction is the decrease in thrust generated by the propellers. Although the looped propeller achieved a lower C_P when compared to the reference propeller, and the effect was furthered by the tubercle variants, the change in C_P was not sufficient to offset the loss of thrust, resulting in the efficiency reducing in both the hover state and forward flight state. T2 was found to have the smallest impact on the efficiency when compared with the baseline looped propeller design.

Overall, the simulations were deemed to be accurate, as the results for the reference propeller matched well with the results of Hanson et al. (2022). The results are also reinforced by the findings of the previous research which found similar reductions in thrust and efficiency for similarly sized looped propeller blades (du Plessis & Bouferrouk, 2024).

With the extent of research conducted on the topic and the limitations discussed, several future research avenues are proposed:

- Further validation should be conducted with physical testing of the models to confirm the findings from the numerical simulations.
- Further simulations should be conducted, using a full Large Eddy Simulation (LES) model to accurately predict the changes to broadband noise emissions.
- Psychoacoustics studies should be conducted to understand how changes to the tones and pitch of the propeller affect the human perception of the noise.
- A parametric study should be conducted to further optimise the shape of the blades and to test the effect of changing the blade's solidity.

References

Cai, J.-C., Qi, D.-T., & Zhang, Y.-H. (2012, 11). A numerical study of the blade passing frequency noise of a centrifugal fan. *ASME International Mechanical Engineer- ing Congress and Exposition, Proceedings (IMECE)*, *12*. doi: 10.1115/IMECE2012-86745

Colpitts, R., & Perez, R. E. (2023). Application of leading-edge tubercles on rotor blades. *AIAA Journal*, *61*. doi: 10.2514/1.J062175

du Plessis, J., & Bouferrouk, A. (2024). Aerodynamic and aeroacoustic analysis of looped propeller blades. In *30th aiaa/ceas aeroacoustics 2024 conference.* Re- trieved from https://arc.aiaa.org/doi/10.2514/6.2024-3156 doi: 10.2514/6.2024-3156

Fahad, R. B., & Talha, T. (2019). Numerical investigation of the effect of leading edge tubercles on propeller performance. *Journal of Aircraft*, *56*. doi: 10.2514/1.C034845

Fish, F., & Lauder, G. (2006, 01). Passive and active flow control by swimming fishes and mammals. *Annu. Rev. Fluid Mech*, *38*, 193-224. doi: 10.1146/annurev.fluid.38.050304.092201

Hanson, L. P., Baskaran, K., Pullin, S. F., Zhou, B. Y., Zang, B., & Azarpeyvand, M. (2022). Aeroacoustic and aerodynamic characteristics of propeller tip geometries. In *28th aiaa/ceas aeroacoustics 2022 conference.* Retrieved from https://arc.aiaa.org/doi/abs/10.2514/6.2022-3075 doi: 10.2514/6.2022-3075

Hsiao, M. L., Zhenbo, L., Kian, M. L., Jinlong, X., & Heow, P. L. (2019). Quieter propeller with serrated trailing edge. *Applied Acoustics*, *146*, 227-236. Retrieved from https://www.sciencedirect.com/science/article/pii/S0003682X18305413 doi: https://doi.org/10.1016/j.apacoust.2018.11.020

Patil, T., Borole, K., & Sanap, S. B. (2013). Noise reduction of centrifugal fan by use of resonator and active noise control technique. *International Journal of Mechanical Engineering (IJME)*. Retrieved from https://www.iaset.us/archives?jname=67_2&year=2013&submit=Search&page=2

Shima, E., Sun, J., Liu, H., Yonezawa, K., & Kaneko, H. (2024). Aeroacoustics, psychoacoustics, and aerodynamic characteristics of innovative looped propellers using catenary curves. In *30th aiaa/ceas aeroacoustics conference.* Retrieved from https://arc.aiaa.org/doi/abs/10.2514/6.2024-3111 doi: 10.2514/6.2024-3111

Shima, E., & Tsutsumi, S. (2023). Preliminary study on innovative loop propellers for quiet evtol. In *Asia rotorcraft forum 2019.* Retrieved from https://www.researchgate.net/publication/368189976_Preliminary_Study_on_Innovative_Loop_Propellers_for_Quiet_eVTOL

Wilkins, R., & Bouferrouk, A. (2023). Numerical framework for aerodynamic and aeroacoustics of bio-inspired uav blades.. Retrieved from https://uwe-repository.worktribe.com/output/10956062 doi: 10.13009/EUCASS2023-948

Xiran, L., Dan, Z., Di, G., Sid, B., Dakun, S., & Sun, X. (2022). Development and progress in aeroacoustic noise reduction on turbofan aeroengines. *Progress in Aerospace Sciences*. Retrieved from https://www.sciencedirect.com/science/article/pii/S037604212100097X doi: 10.1016/j.paerosci.2021.100796

Zang, B., Hanson, L., Stoltz, A., Ho, W., Liu, X., & Azarpeyvand, M. (2023, June 8). Numerical and experimental investigation of propeller noise with trailing-edge serrations. In *Aiaa aviation 2023 forum.* United States: American Institute of Aeronautics and Astronautics Inc. (AIAA). (2023 AIAA Aviation Forum ; Conference date: 12-06-2023 Through 16-06-2023) doi: 10.2514/6.2023-3835